Peptidic Determinants and Structural Model of Human NDP Kinase B (Nm23-H2) Bound to Single-Stranded DNA†

Sharona Raveh,‡ Joëlle Vinh,§ Jean Rossier,§ Fabrice Agou,*,‡ and Michel Véron‡

Unité de Régulation Enzymatique des Activités Cellulaires, Institut Pasteur, CNRS-FRE 2364, 25−28 rue du Docteur Roux, 75724 Paris Cedex 15, France, and Laboratoire de Neurobiologie et Diversité Cellulaires, Ecole Supérieure de Physique et Chimie Industrielles de la Ville de Paris, CNRS UMR 7637, 75231 Paris Cedex 05, France

Received May 12, 2000; Revised Manuscript Received January 10, 2001

ABSTRACT: Isoform B of human NDP kinase (NDPK-B) was previously identified as a transcription factor stimulating in vitro and ex vivo the transcription of the c-*myc* oncogene, which involves this enzyme in carcinogenesis. We have studied the enzymatic properties of NDPK-B in the presence of several single-stranded oligonucleotides. We show that the oligonucleotides are competitive inhibitors of the catalytic activity, indicating that the active site acts as a binding template for the anchorage of the oligonucleotide. Furthermore, the presence of a guanine at the 3′-end of several different aptamers increases its affinity 10-fold. To define the surface of the protein contacting the DNA within the nucleoprotein complex, we used single nanosecond laser pulses as the cross-linking reagent and MALDI-TOF mass spectrometry to identify cross-linked peptides purified from proteolytic digests of the cross-linked complex. Using 11-mer and 30-mer single-stranded oligonucleotides, the same three different nucleopeptides were identified after irradiation of the complexes, indicating a common binding mode for these two aptamers. Taken together, these results allowed us to propose a structural model of NDPK-B bound to single-stranded DNA.

Nucleoside diphosphate kinases are ubiquitous enzymes which catalyze the transfer of the γ-phosphate from a nucleoside triphosphate (NTP) to a nucleoside diphosphate (NDP) by a ping-pong mechanism which involves the formation of a phosphohistidine intermediate (*1*). In general, NDP kinases display little specificity for the nucleobase, although a preference for GDP was reported (*2*, *3*). Most NDP kinases are made of small ≈17 kDa subunits arranged in an oligomer. The crystal structures of NDP kinases from several species have been determined at high resolution. All known NDP kinases from eukaryotes are hexamers made of two trimers or three dimers (*4*, *5*). Extensive biochemical (*6*) and structural studies of NDP kinase in the presence of several NDP (*7*, *8*) or nucleotide analogues (*9*) have allowed a precise description of the active site of the transition state (*10*). In all cocrystals, the conformation of the base in the active site is very similar. The base stacks on the aromatic ring of a Phe 60 and is wedged between the side chains of strictly conserved Phe 60 and Val 112 (human numbering). Although each subunit contains one active site, the oligomeric state is essential for catalytic activity since dimeric mutants of the NDP kinase from *Dictyostelium* are lacking catalytic activity (*11*).

In humans, several NDP kinases, including NDPK-A (*12*), NDPK-B[1] (*13*), DR-*nm23* (*14*), *nm23*-H4 (*15*), and *nm23*-H5 (*16*) which are part of the *nm23* gene family (*19*), have been identified. *nm23*-H_1 and *nm23*-H_2 respectively encode NDPK-A and NDPK-B, two isozymes of NDP kinase which are abundant in the mammalian cells (*17*). Although they are highly homologous (88%), NDPK-A and NDPK-B differ in a number of ways. Thus, type A subunits have a very acidic pI while type B subunits are very basic (*17*), and they display very different stability properties. Indeed, the hexamer of human NDPK-A is stable even at a high urea concentration (5 M) as is the NDP kinase from the lower eukaryote *Dictyostelium discoideum*, whose structure was the first to be determined after its crystallization (*4*) [NDPK-A (*18*)]. In contrast, NDPK-B is less stable, although it is also found as a hexamer in solution (*20*).

Human NDPK-B was reported as a transcription factor for the c-*myc* oncogene (*21*). It is able to stimulate the transcription of the human c-*myc* gene ex vivo (*22*, *23*) and in vitro (*21*) via the specific recognition of a nuclease hypersensitive cis-activating element, termed NHE. This

† This work was performed in part with grants from Association pour la Recherche sur le Cancer (ARC) and Agence Nationale de Recherches sur le Sida (ANRS).

* To whom correspondence should be addressed. Telephone: (33-1) 45 68 83 80. Fax: (33-1) 45 68 83 99. E-mail: fagou@pasteur.fr.

‡ Unité de Régulation Enzymatique des Activités Cellulaires, Institut Pasteur, CNRS-FRE 2364.

§ Laboratoire de Neurobiologie et Diversité Cellulaires, CNRS UMR 7637.

[1] Abbreviations: NDPK-B, isoform B of human NDP kinase; NDP kinase, nucleoside diphosphate kinase; MALDI-TOF MS, matrix-assisted laser desorption ionization time-of-flight mass spectrometry; Dd, *Dictyostelium discoideum*; TLC, thin-layer chromatography; RP-HPLC, reversed-phase high-performance liquid chromatography; SA, sinapinic acid; DHB, 2,5-dihydroxybenzoic acid; 3-HPA, 3-hydroxypicolinic acid; 6ATT, 6-aza-2-thiothymine; 2-ABA/NA, mixture of 2-aminobenzoic acid and nicotinic acid; DAHC, diammonium hydrogen citrate; TFA, trifluoroacetic acid; DTE, dithioerythritol; RNP, ribonucleoprotein domain; hnRNP-K, heterogeneous nuclear ribonucleoprotein K; NHE, nuclease hypersensitive element.

10.1021/bi001085j CCC: $20.00
Published on Web 04/26/2001

activity is conserved in a catalytically inactive mutant (*24*, *28*). The Nm23-H2/NDPK-B has been located in the nucleus in association with chromatin (*29*), and confocal microscopy has shown the presence of NDPK-B but not of NDPK-A in the nucleus (*30*). In a previous study, we have investigated the DNA binding activity of human NDPK-B using a combination of filter binding assays and fluorescence spectroscopy. We showed that the binding which has little sequence specificity occurs with single-stranded DNA (*20*). Interestingly, the polypurine/polypyrimidine sequence composing this NHE element can adopt a non-B duplex DNA conformation compatible with the H conformation of DNA (*25*, *26*) or with intramolecular tetraplexes (*27*).

Mass spectrometry has been used to localize the interaction site(s) of proteins photochemically linked to oligonucleotides and to identify the peptide−oligomer complexes after proteolysis of the cross-linked protein (*50*, *51*). In this paper, we measured the binding constants for a series of aptamers binding to NDPK-B, and we combined the photo-cross-linking of the protein to the oligonucleotide by nanosecond-pulsed UV laser (*32*) and matrix-assisted laser desorption ionization (MALDI) mass spectrometry. We show that the active site of NDPK-B contributes to DNA binding, and we identify several peptidic determinants of the protein contacting the oligonucleotide. These results allowed the building of a molecular model of NDPK-B bound to an 11-mer oligonucleotide.

EXPERIMENTAL PROCEDURES

Materials. ATP and [^{14}C]ADP were obtained from Roche Molecular Biochemicals and Amersham Pharmacia Biotech. Nicotinic acid (NA), ammonium bicarbonate, and diammonium hydrogen citrate (DAHC) were purchased from Sigma. 2-Aminobenzoic acid (2-ABA), 3-hydroxypicolinic acid (3-HPA), 2,5-dihydroxybenzoic acid (DHB), sinapinic acid (SA), and 6-aza-2-thiothymine (6ATT) were from Aldrich. Spermine dihydrate was from Fluka. Zwittergent 3-16 was from Calbiochem. Endoproteinase Lys-C (sequencing grade), 3′-specific snake venom phosphodiesterase I, and 5′-specific calf spleen phosphodiesterase were from Roche Molecular Biochemicals. All oligonucleotides were obtained from Eurogentec. Dinucleotides were from Sigma or Institut Pasteur. All oligonucleotides were gel-purified following protocols derived from Sambrook et al. (*33*). Short oligonucleotides (10−11 polymers) were precipitated as described previously (*20*). Concentrations of all oligonucleotides and dinucleotides were calculated from their absorbance at 260 nm according to the nearest approximations of Puglisi and Tinoco (*34*).

Enzyme Purification and Activity Assays. The different NDP kinases, namely, *D. discoideum* (Dd) NDPK, NDPK-A, and NDPK-B, were expressed in *Escherichia coli* and purified as described previously (*6*, *20*, *35*). All proteins were purified to homogeneity and analyzed by sodium dodecyl sulfate−polyacrylamide gel electrophoresis (SDS−PAGE) after Coomassie Blue staining. Protein concentrations were determined either by the Bradford method or by measuring the absorbance at 280 nm using an extinction coefficient of 1.24, 1.25, or 0.55 for a 1 mg/mL solution of NDPK-B, NDPK-A, or Dd-NDPK, respectively. In all experiments, the enzyme concentration was expressed as the concentration of monomers. NDP kinase activity was measured according to the method described in ref *36* by following the formation of [^{14}C]ATP from [^{14}C]ADP (0.1 mM) in the presence of cold ATP (200 or 400 μM) in DNA binding buffer (DB buffer) consisting of 20 mM potassium phosphate (pH 7.0), 75 mM potassium chloride, 5 mM magnesium chloride, and 1 mM DTE. For determination of the K_i values of different aptamers on the catalytic activity, NDPK-B (20 nM) was preincubated for 5 min at 20 °C in the presence of increasing concentrations of oligonucleotide or dinucleotide (from 3 nM to 1.2 μM). The activity assay was started by adding 4.5 μL of this preincubation mixture to 10 μL of reaction mix containing DB buffer and the substrates ADP and ATP as indicated above. The reaction was stopped by adding 3 μL aliquots of the assay mix to 2 μL of stop solution consisting of 0.7 M formic acid and ADP and ATP (10 mM each). Radioactive ATP and ADP were then separated by thin-layer chromatography (TLC) with a UV indicator. The TLC plates were developed with 1 M formic acid and 1.5 M LiCl, and the radioactive products were quantified by PhosphorImage densitometry using ImageQuant software (Molecular Dynamics). Points taken after reaction for 2, 4, and 6 min showed that the rate of product accumulation was constant in this time range, allowing determination of the initial velocity. The data are presented using the Dixon representation in which the reciprocal of the reaction rate is plotted as a function of inhibitor concentration at two different fixed ATP concentrations (200 or 400 μM depending on the experiment). For a given inhibitor, the intercept of the two straight lines allowed us to calculate the value of K_i for the inhibitor (see Figure 1).

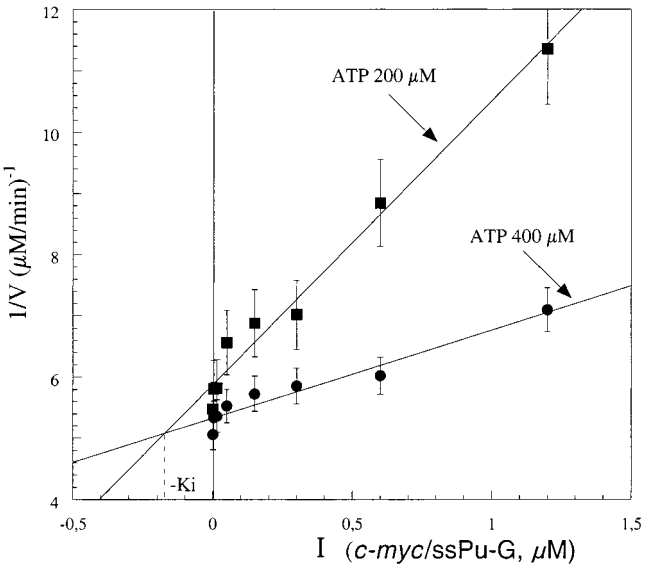

FIGURE 1: Competitive inhibition of ATP synthesis by a ssDNA aptamer. Initial rates were measured as described in Experimental Procedures, in the presence of 200 (■) or 400 μM (●) ATP. The aptamer that was used (c-*myc*−ssPu-G) was varied from 0.003 to 1.2 μM. The reaction rates are plotted according to the Dixon representation. The intercept of the two straight lines that are obtained is above the [I] axis, indicating that the ssDNA aptamer is a competitive inhibitor. The value of K_i is computed from the abscissa of the intersection (K_i = 170 nM in the example shown).

Fluorescence Studies. The binding of oligonucleotides or dinucleotides to NDP kinase was assessed as described previously by monitoring the variation of the intrinsic

fluorescence of the protein (*20*). The fluorescent measurements were performed on a PTI spectrofluorometer Quantamaster at 20 °C in DNA binding (DB) buffer containing 5% glycerol to stabilize the fluorescence signal. The fluorescence excitation and emission wavelengths were 304 and 340 nm, respectively. A typical titration curve was obtained by adding a variable amount of aptamer to a constant concentration of NDP kinase. Data were fitted to the Langmuir binding equation where K_D represents the dissociation constant using a nonlinear regression analysis with KaleidaGraph software (Synergy Software, Reading, PA) as described previously (*20*). The stoichiometry of binding sites (*n*) was determined graphically using a NDPK-B concentration higher than the expected K_D (see ref *20*).

UV Laser Cross-Linking of Radioactively Labeled Oligonucleotides to NDPK-B. Two single-stranded poly(dT) oligonucleotides bearing a guanine at their 3′-end were used in the UV laser cross-linking experiments, an 11-mer d[T_{10}-G] and a 30-mer d[T_{29}-G]. For convenience, these oligonucleotides will generally be termed "11-mer" and "30-mer", respectively. The single-stranded oligonucleotides were 5′-end radiolabeled with T4 polynucleotide kinase and [γ-^{32}P]ATP (4500 Ci/mmol) and separated from free [γ-^{32}P]-ATP via denaturing 20% polyacrylamide gel electrophoresis. Complexes of labeled oligonucleotide (17 nM) with variable concentrations of NDPK-B (0.05−6 μM) were formed for 30 min at 20 °C in 10 μL of DB buffer. Following incubation for 20 min, the samples were irradiated with a pulsed Nd:YAG laser (Spectra Physics) as described in ref *32* with an average fluency of 30 mJ/pulse (10^{17} photons/pulse, at 266 nm, 5 ns pulses). After UV irradiation, the samples were analyzed by 12% SDS−PAGE. The gel was then dried and scanned using a PhosphoImager (Molecular Dynamics). The dissociation constant (K_D) of the cross-linked complex was computed using a hyperbolic extrapolation.

Experiments of UV laser cross-linking in the presence of different concentrations of urea were performed as follows. Samples of NDPK-B (6 μM) were separately dialyzed at 20 °C overnight against several DB buffers (2 × 500 mL) without or with 2−6 M urea. The dialyzed samples were then incubated with 17 nM [γ-^{32}P]d[T_{10}-G] for 30 min prior to UV laser cross-linking and analysis via 12% SDS−PAGE.

For the exonuclease protection assay, the 11-mer oligonucleotide was either 5′-end labeled as mentioned above or 3′-end radiolabeled with terminal deoxynucleotidyltransferase and [α-^{32}P]dGTP [3000 Ci/mmol (*33*)]. The radiolabeled oligonucleotides were separated from free [α-^{32}P]dGTP via 20% polyacrylamide gel electrophoresis under denaturing conditions. After cross-linking with a large excess of protein (17.5 nM oligonucleotide and 6 μM NDPK-B), the mixture was treated with exonuclease, either with 3′-specific snake venom phosphodiesterase I (1.66 μg/mL) or with 5′-specific calf spleen phosphodiesterase (0.4 μg/mL) at 25 °C for different times, as indicated in Figure 4. The samples were then boiled for 2 min and analyzed by 12% SDS−PAGE.

Preparation of Proteolytic Samples for MALDI Analysis. Protein samples irradiated or not irradiated (6 μM in 250 μL) were incubated overnight at 37 °C, with or without nonradioactive aptamer, with the endoproteinase Lys-C (0.05 μg/mL) in 50 mM Tris-HCl buffer (pH 8.5) containing 0.2 M guanidine hydrochloride and 1 mM EDTA. The samples were concentrated 10 times under vacuum and resuspended twice in 100 μL of water containing 0.1% (v/v) Zwittergent 3-16. In some experiments, the digestion mixture of peptides and nucleopeptides was directly analyzed by MALDI-TOF mass spectrometry (see below). Alternatively, the mixture was separated by reversed-phase liquid chromatography (RP-HPLC) using a SMART system (Amersham Pharmacia Biotech). For this, the proteolytic digest (100 μL) was loaded onto a C2/C18 reverse-phase column (μRPC C2/C18 SC 2.1/10, Amersham Pharmacia Biotech) equilibrated in 5 mM potassium phosphate (pH 7.0) and eluted at a rate of 200 μL/min with a 10 mL linear gradient of acetonitrile (from 0 to 70%). Cross-linked peptides were detected using three simultaneous wavelengths at 214, 254, and 280 nm by comparison of chromatographic profiles for the digest of the protein and the oligonucleotide with or without irradiation (solid and dotted lines in Figure 6A, respectively) or with the digest of protein irradiated alone. Fractions containing cross-linked peptides (200 or 100 μL) were frozen, and then concentrated under vacuum to a final volume of ∼10 μL before MALDI-TOF analysis.

Peptide Identification Using MALDI-TOF MS. As previously reported (*37*), simultaneous desorption and ionization of peptides and oligonucleotides is challenging. We tried several matrix preparations, such as the classical dried droplet method with sinapinic acid (SA), 2,5-dihydroxybenzoic acid (DHB), 3-hydroxypicolinic acid (3-HPA), 6-aza-2-thiothymine (6ATT), and a mixture of 2-aminobenzoic acid and nicotinic acid (2-ABA/NA), with ammonium bicarbonate or diammonium hydrogen citrate (DAHC), with or without spermine as a comatrix. The best reproducible results were obtained using an 8:2 (w/w) mixture of 2-ABA and NA which allows the simultaneous analysis of both the oligonucleotide and the peptides from the same spot. Spermine was used as a comatrix to improve the cocrystallization of oligonucleotide with the matrix as described in ref *38*. Ammonium salts were added as competitors for alkali metal ions (*39*). The samples were concentrated under vacuum, and then diluted in 100 mM DAHC to reach a total concentration of 1 pmol/μL. Fresh saturated 8:2 (w/w) matrix 2-ABA/NA solution in a 1:1 (v/v) acetonitrile/100 mM aqueous DAHC mixture were prepared extemporaneously. The clean stainless steel MALDI target was sonicated for 30 min in a saturated ammonium bicarbonate aqueous solution and dried under vacuum before use. Then 0.5 μL of 50 mM spermine was spotted onto the target and mixed first with 0.5 μL of the sample solution, and then with 0.5−1 μL of the supernatant of the matrix solution. The preparation was dried under low pressure. Mass spectra were recorded in MS mode with a Voyager STR MALDI-TOF mass spectrometer (PerSeptive Biosystems Inc., Framingham, MA) equipped with a delayed extraction device and a nitrogen laser (λ = 337 nm, 3 ns wide pulse at 20 Hz, laser power set just above the desorption threshold). The spectra were acquired in linear and negative mode (2 m total flight length) to obtain the best signal-to-noise ratio. The delayed extraction time was set between 100 and 150 ns, and the accelerating voltage was set at 21 kV, with a grid voltage of 96% of this value. About 75 shots were averaged for each acquisition. External calibration was performed with a mixture of neurotensin and adrenocorticotropin (18−39 clip), with monoisotopic masses for $[M + H]^+$ of 1672.92 and 2465.20 Da, respectively.

Structural Modeling of the d[T_{10}-G]−NDPK-B Complex. The modeling of d[T_{10}-G] complexed to NDPK-B was based on the known X-ray structure of NDPK-B bound to GDP [PDB entry 1NUE (*5*)]. The single-strand aptamer was built using the Insight II program (Molecular Simulations, San Diego, CA). The model was constructed by docking manually the phosphate backbone according to the footprintings shown in Figure 8 with constraints to maintain the G 3′-end superimposed to the G of the GDP substrate. During docking, unfavorable and favorable contacts of NDPK-B atoms were searched by calculating electrostatic and van der Waals interaction energies using the Docking module of Insight II. The resulting model we found with the minimal energy is shown in Figure 8.

RESULTS

A Single-Strand Aptamer Is a Competitive Inhibitor of NDPK-B Catalytic Activity. First, we performed steady-state kinetics studies to test if the oligonucleotide acts as a competitive inhibitor in the catalytic reaction. Figure 1 shows the initial rates of ATP formation from ADP for a series of experiments using ATP as the phosphate donor at two different concentrations (200 and 400 μM). ADP was used as the substrate because its intracellular concentration is the highest among the ribonucleotide pool and the [ADP]/K_m ratio indicates that it is the most natural ribonucleotide substrate in mammals (*3*, *54*). In each experiment, the concentrations of radiolabeled ADP and ATP were kept constant while the single-strand aptamer concentration playing the role of an inhibitor (I) was varied from 3 to 1200 nM. We first assayed the c-*myc*−ssPu-G aptamer corresponding to a single nucleotidic motif of NHE element mimicking the noncoding strand of the cis-activating element of the c-*myc* gene (ref *40* and Table 1). The Dixon plot representation of the data ($1/v$ vs [I]) shows a linear dependence of $1/v$ on aptamer concentration [I], indicating that the inhibition is not cooperative. The intercept of the two lines corresponding to the two ATP concentrations (200 and 400 μM) is located above the [I] axis, showing that the aptamer acts as a competitive inhibitor. The abscissa of the intersection point allows us to determine an inhibition constant (K_i) of the c-*myc*−ssPu-G aptamer for NDPK-B of 170 nM, indicating a very strong competitive inhibition of NDPK-B catalytic activity by this aptamer.

A Guanine at the 3′-End of the Aptamer Greatly Increases Its Binding Affinity. The crystal structure of hexameric NDPK-B with bound GDP in its active site shows a specific hydrogen bound between the amino group of the guanine and the protein (*5*). To test whether the nature of the base at the extremity of the aptamer could influence its binding affinity for NDPK-B, we measured the inhibitory power (K_i) of several single-strand aptamers differing only by the base at their 3′- or 5′-end. As shown in Table 2, the presence of a guanine at the 3′-end of the oligonucleotide increased its inhibitory efficiency by more than 10-fold. Thus, K_i values for NDPK-B are 10-fold higher for d[C_{10}-G] than for the homopolymer d[C_{10}], while the presence of the guanine at the 5′-end had no effect. Low K_i values were also found for other oligonucleotides with a guanine at their 3′-end, like the d[T_{10}-G] oligonucleotide or the c-*myc*−ssPu-G aptamer corresponding to the purine strand of the c-*myc* NHE element also used in Figure 1. The importance of the presence of a guanine at the 3′-end of the aptamer was also demonstrated by measuring the binding activity by fluorescence titration. The dissociation constant K_D was 6-fold lower for d[C_{10}-G] than for the homopolymer d[C_{10}] (Table 2). The stoichiometry of binding (0.4 aptamer per subunit) corresponded to about 3 oligonucleotides bound per hexamer of NDPK-B, suggesting that other protein determinants not included in the active site were involved in the binding.

Although the decreases are slightly less pronounced, the presence of a guanine at the 3′-end of a dideoxyribonucleo-

Table 1: RNA and DNA Aptamers Used in This Study[a]

Name	Length (-mer)	sequence (5′ → 3′)
Oligonucleotides		
d$(C)_{10}$	10	CCCCCCCCCC
d[C_{10}-G]	11	CCCCCCCCCCG
d[G-C_{10}]	11	GCCCCCCCCCC
d[T_{10}-G]	11	TTTTTTTTTTG
d[T_{29}-G]	30	TTTTTTTTTTTTTTTTTTTTTTTTTTTTTG
c-*myc*/ssPu-G	11	TGGGGAGGGTG
Dinucleotides		
d(AG)	2	AG
d(GA)	2	GA
r(AG)	2	AG
r(GA)	2	GA
r(GG)	2	GG
r(AA)	2	AA

[a] c-*myc*/ssPu-G corresponds to a single DNA motif contained in the cis-activating element of the c-*myc* gene (*21*, *49*).

Table 2: Binding of Single-Strand Aptamers to NDPK-B[a]

single-strand aptamer	K_i (nM)	K_D (nM)	stoichiometry per monomer
polynucleotide			
d$(C)_{10}$	2700 ± 200	120 ± 30	0.4
d[C_{10}-G]	230 ± 20	20 ± 10	0.4
d[G-C_{10}]	3100 ± 300	nd[b]	−
d[T_{10}-G]	300 ± 20	nd	−
c-*myc*/ssPu-G	170 ± 15	20 ± 10	0.4
dinucleotide			
r(AG)	nd	80 ± 10	1
d(AG)	280 ± 30	100 ± 20	1
d(GA)	2500 ± 100	700 ± 80	1

[a] Inhibition constants (K_i) for NDPK-B in the ATP−ADP exchange reaction were derived from the abscissa of the intercept of inhibition curves of the corresponding aptamer at 200 and 400 μM ATP as shown in Figure 1. Dissociation constants were measured by monitoring the intrinsic fluorescence of the protein in the presence of a variable concentration of aptamers as described previously (*20*). Stoichiometry values result from the analysis of two independent saturation curves performed with 0.5 and 2 μM NDPK-B. [b] nd, not determined.

Table 3: Dissociation Constants of Diribonucleotides for Several Eukaryotic NDPKs Measured by Fluorescence Titration

	K_D		
diribonucleotide	NDPK-A (nM)	NDPK-B (nM)	Dd-NDPK (nM)
r(AG)	3000 ± 400	80 ± 10	11000 ± 3000
r(GA)	14000 ± 4000	500 ± 70	180000 ± 15000
r(AA)	10000 ± 1000	300 ± 50	15000 ± 5000

tides or a diribonucleotides also reduced both its K_i and K_D for NDPK-B (Table 2). However, the stoichiometry was then of one dinucleotide bound per subunit, indicating that in the case of these very short oligomers, the binding involved the six active sites within the hexamer. The dissociation constants of diribonucleotides for different NDP kinases were also determined using fluorescence titration. We compared the binding to NDPK-B to the binding to NDPK-A, a highly homologous human isozyme, as well as to the enzyme isolated from *D. discoideum*. As shown in Table 3, there is a strong preference for binding to NDPK-B of the three diribonucleotides that were tested [r(AG), r(GA), and r(AA)], with a K_D 30- and 100-fold lower than for NDPK-A and for *Dictyostelium* NDP kinase, respectively. With NDPK-A, some effects of the presence of a guanine at the 3′-end could be seen, while no such correlation could be established in the case of *Dictyostelium* NDP kinase (see the Discussion).

Characterization of the ssDNA−NDPK-B Complex by Laser UV Cross-Linking. UV laser irradiation was used to cross-link NDPK-B and a single-strand aptamer under experimental conditions minimizing the nonspecific DNA−protein interactions. These include the use of neutral pH, an ionic strength of >100 mM, and the presence of a weak chaotropic salt such as potassium chloride (*20*). We used a single-strand d[T_{10}-G] oligonucleotide made of a poly(dT) bearing a guanine at its 3′-end because the cross-linking efficiency is optimal with a poly(dT) (*32*). A given concentration (5 nM) of ^{32}P-radiolabeled oligonucleotide was incubated in DB buffer with a variable concentration of NDPK-B (0.05−6 μM) and irradiated under UV laser light at 266 nm, as described in Experimental Procedures. The analysis of the sample by SDS−PAGE (Figure 2) shows only one radiolabeled protein band corresponding to the covalent 22.5 kDa nucleoprotein complex formed upon irradiation. Controls included the autophosphorylation of NDPK-B in the presence of [γ-^{32}P]ATP with (Figure 2, lane 6) or without UV laser irradiation (data not shown). This complex corresponded to the adduct composed of one subunit bound to one oligonucleotide as shown by its apparent molecular mass of 22.5 kDa. When NDP kinase was irradiated in the absence of oligonucleotide (Figure 2, lane 6), a minor polypeptide band with a molecular mass of 35 kDa was also present, probably corresponding to a dimer of NDPK-B formed by protein cross-linking between two adjacent subunits within a hexamer. This band can also be seen with the cross-linked complex, when the gel is heavily loaded (see Figure 3A).

For a given oligonucleotide concentration, the amount of nucleoprotein complex increased with protein concentration (Figure 2A). The measurement of the amount of radioactivity of the complex by PhosphorImage densitometry (Figure 2B) allowed us to quantify oligonucleotide binding and to compute an apparent dissociation constant of 0.15 μM with a complex stoichiometry of two monomers bound per oligonucleotide. These results are remarkably similar to those obtained above by fluorescence titration. It should be noted that only 4% of the oligonucleotide was cross-linked at a saturating concentration of NDPK-B. This low efficiency is in accordance with the theoretical cross-linking of protein to nucleic acids using UV laser pulses of 5 ns at 266 nm (*32*). Reverse titration by the same method using a constant concentration of NDPK-B (1 μM) and varying concentrations of radiolabeled oligonucleotide (5 nM to 8 μM) gave similar results, and allowed us to confirm a stoichiometry of the complex corresponding to three oligonucleotides bound per hexamer (data not shown). When a similar experiment was performed using the same radiolabeled oligonucleotide and NDPK-A even at a larger excess, no covalent complex could be seen (Figure 3A), demonstrating the specificity of NDPK-B for the aptamer−protein interaction.

We also investigated the effect of urea on the formation of the complex (Figure 3B). NDPK-B was preincubated in the presence of various concentrations of urea before cross-linking and SDS−PAGE analysis of the reaction products. Increasing concentrations of urea strongly diminish the level of photoadduct formation (compare lanes 2−5). No cross-linking was observed at a high urea concentration (6 M), indicating that a denatured conformation of NDPK-B is unable to produce specific DNA−protein contacts.

To evaluate whether the free end of the bound oligonucleotide was buried inside the protein, we performed a series of experiments. The complex obtained by UV laser irradiation of the labeled oligonucleotide (either at its 5′-end or at its 3′-end) was digested with 3′ → 5′ exonuclease (Figure 4A) or with 5′ → 3′ exonuclease (Figure 4B) before SDS−PAGE analysis. The oligonucleotide alone radiolabeled at either the 5′- or 3′-end is rapidly digested with 3′ → 5′ exonuclease (see "free oligo" band in Figure 4A, lanes 1 and 7) or with 5′ → 3′ exonuclease (Figure 4B, lanes 1 and 3). In contrast, the degradation of the covalent complex is significantly protected when nuclease attack was performed with 3′ → 5′ exonuclease (lane 2; lanes 5 and 6 in Figure 4A). Furthermore, a significant degradation of the free oligonucleotide is observed upon nuclease incubation for 2 min (Figure 4A, lane 6) or 6 min (Figure 4A, lane 5), whereas no hydrolysis of the covalent complex could be detected when the oligonucleotide was labeled at the 5′-end. The pattern of the covalent complex was different when nuclease digestion was carried out with 5′ → 3′ exonuclease. Indeed, no protection was observed when the oligonucleotide was labeled at the 5′-end (Figure 4B, lanes 1 and 2), while a partial protection is observed with the oligonucleotide labeled at the 3′-end. These results strongly support the hypothesis that the 3′-end of a single-strand aptamer bound to NDPK-B is buried inside the hexameric protein, leading to a partial protection against exonuclease attack.

Purification and Identification of Covalent Photo-Cross-Linked Complexes. To identify the peptidic determinants of NDPK-B involved in single-strand DNA binding, we used a novel strategy by combining UV laser cross-linking and matrix-assisted laser desorption ionization time-of-flight mass spectrometry (MALDI-TOF MS). We first attempted to identify the peptides and nucleopeptides directly from a proteolytic digest with endoproteinase Lys-C of the cross-linked mixture of NDPK-B and the 11-mer d[T_{10}-G]. Figure 5 shows the MALDI-TOF spectrum of such a digest. Eleven

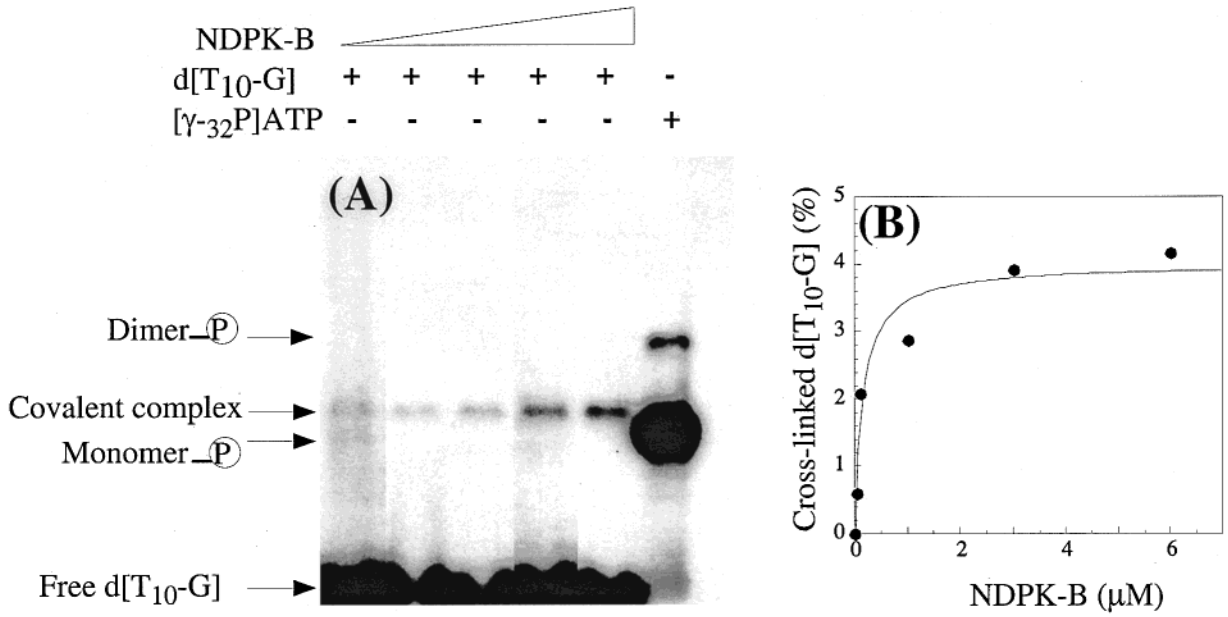

FIGURE 2: Laser-mediated UV cross-linking of the NDPK-B to d[T_{10}-G]. (A) Purified [^{32}P]d[T_{10}-G] (17 nM) was incubated with variable amounts of NDPK-B (lane 1, 0.05 μM; lane 2, 0.1 μM; lane 3, 1 μM; lane 4, 3 μM; and lane 5, 6 μM) in DB buffer and cross-linked with a UV laser, and the mixture was analyzed by SDS−PAGE. The radioactivity at the bottom of the gel corresponds to the free oligonucleotide. In lane 6, NDPK-B was incubated in the presence of [γ-^{32}P]ATP in the absence of added oligonucleotide. Under these conditions, the protein instantly autophosphorylates on a histidine residue due to the ping-pong catalytic mechanism (*1*). The phosphorylated protein was further exposed to a pulse of UV light in the absence of oligonucleotide before electrophoresis. The phosphohistidine formed is stable under the conditions of the experiment, and almost all the [γ-^{32}P]ATP that was added was transferred to the protein. The phosphorylated protein represented is slightly retarded and migrates as a polypeptide with an apparent molecular mass of 19.7 kDa (compared to 17 kDa for the unphosphorylated enzyme). (B) The bands corresponding to the nucleoprotein complex in panel A were quantified by PhosphorImage densitometry. The solid curve represents the nonlinear least-squares fit of the binding equation corresponding to an apparent binding constant (K_D) of 0.15 μM.

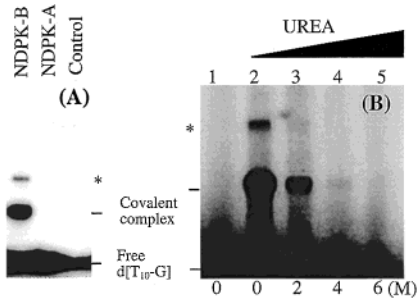

FIGURE 3: Specificiy of the cross-linking reaction. (A) Laser UV cross-linking of NDPK-B and NDPK-A. [^{32}P]d[T_{10}-G] (17 nM) was incubated for 30 min at 20 °C in DB buffer alone (control) or with either NDPK-B (6 μM) or NDPK-A (12 μM) prior to laser UV irradiation and SDS−PAGE. (B) Effect of urea on photo-cross-linked complex formation. Samples of NDPK-B (6 μM) were dialyzed overnight at 20 °C in DB buffer containing urea concentrations from 0 to 6 M (lanes 2−5). The [γ^{32}P]d[T_{10}-G] (17 nM) was then incubated without (lane 1) or with different samples of protein dialyzed for 30 min prior to laser UV cross-linking and analysis by 12% SDS−PAGE. A minor fraction of the cross-linked complex (*) formed by protein cross-linking between two adjacent subunits within an hexamer is indicated.

peptides could be identified (noted by the number of their first and last amino acids), which correspond to the expected number of peptides given the specificity of Lys-C which cleaves after lysine residues. The accuracy of the determination of the experimental masses of these peptides allowed an unambiguous identification for all peptides (Table 4). In addition, the spectrum in Figure 5 exhibited two additional peaks. The peak denoted d[T_{10}-G] corresponds to the free oligonucleotide (Table 4). Although very small, a peak corresponding to a mass of 5542 Da could also be identified (Figure 5, inset). We identified this peak to the nucleopeptide complex because it was the only one missing when the mixture of NDPK-B and oligonucleotide was not subjected to UV laser irradiation (data not shown). The difference in mass with the added masses of residues E129−K143 and of the oligonucleotide (5205 Da) (see Table 4) is most likely due to the presence of potassium adducts (see the Discussion).

In a further experiment, we analyzed by RP-HPLC the Lys-C digestion of the NDPK-B/oligonucleotide mixture before and after irradiation. As shown in Figure 6A, irradiation generated a single new peak (noted peak I), which exhibited the spectral specifications of a nucleopeptide (not shown) as indicated by the ratio of absorbency at 254 and 280 nm. When the fractions of the HPLC column shown in Figure 6A were analyzed by mass spectrometry, the elution position of residues E129−K143 could be identified without ambiguity (see Figure 6A). Figure 6B displays the mass spectrum corresponding to peak I. The spectrum exhibits one clear peak corresponding to a complex between residues E129−K143 and the oligonucleotide (denoted "complex" in Figure 6B, *m*/*z* 5553). Both the free oligonucleotide (denoted "oligonucleotide" in Figure 6B, *m*/*z* 3308) and the free peptide of residues E129−K143 [denoted "peptide (E129−K143)" in Figure 6B, *m*/*z* 1895] were also observed in the spectrum. Since both the free oligonucleotide and the free peptide of residues E129−K143 are well separated from peak I (see Figure 6A), it is clear that the nucleopeptide has experienced cleavage. Oligonucleotide adducts of spermine and potassium were also detected, which is expected since the whole cross-linking protocol was run in the presence of

Table 4: Comparison between Theoretical and Experimental Masses of Endoproteinase Lys-C Digest Products from Photo-Cross-Linked NDPK-B and d[T_{10}-G]

peptidic fragment		average mass $[M - H]^-$	
sequence	positions	theoretical	experimental
TGRVMLGETNPADSKPGTIRGDF-CIQVGRNIIHGSDSVK	86−124	4126.6	4124.1
ANLERTFIAIKPDGVQRGLVGEIIK[a]	2−26	2737.2	2737.6
YMNSGPVVAMVWEGLNVVK	67−85	2092.5	2092.5
EISLWFKPEELVDYK	129−143	1895.2	1895.2
FLRASEEHLK	40−49	1228.4	1228.2
DRPFFPGLVK	57−66	1174.4	1174.5
SCAHDWVYE	144−152	1108.2	1108.2
GFRLVAMK	32−39	920.2	919.9
QHYIDLK	50−56	915.1	914.9
RFEQK	27−31	705.8	705.2
SAEK	125−128	432.4	431.9
nucleotidic or nucleopeptidic fragment			
d[T_{10}-G]		3309.2	3310.5
d[T_{10}-G]-^{129}EISLWFKPEELVDYK^{143}		5205.4	5542.8

[a] Methionine initiator is posttranslationally removed in vivo (*19*).

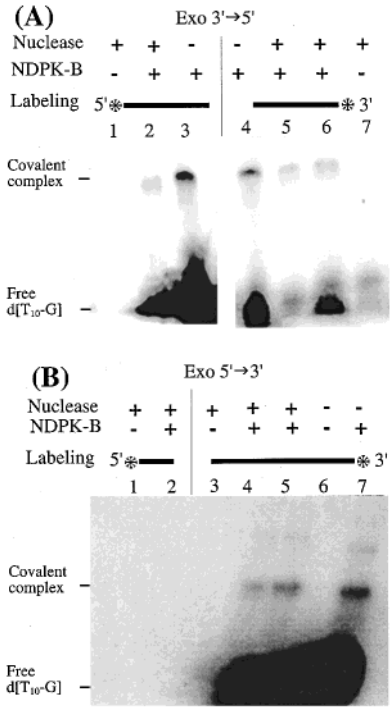

FIGURE 4: Nuclease protection assay. Partial protections of the oligonucleotide−NDPK-B complex from the degradation by snake venom nuclease (A, exo 3′ → 5′) or by calf spleen phosphodiesterase (B, exo 5′ → 3′) were performed with a d[T_{10}-G] labeled at either the 5′-end (A, lanes 1−3; B, lanes 1 and 2) or its 3′-end (A, lanes 4−7; B, lanes 3−7). Different digestion times were used: (A) 5 min for lanes 1, 2, 5, and 7 and 2 min for lane 6 and (B) 2 min for lanes 1 and 2, 5 min for lanes 3 and 4, and 1 min for lane 5.

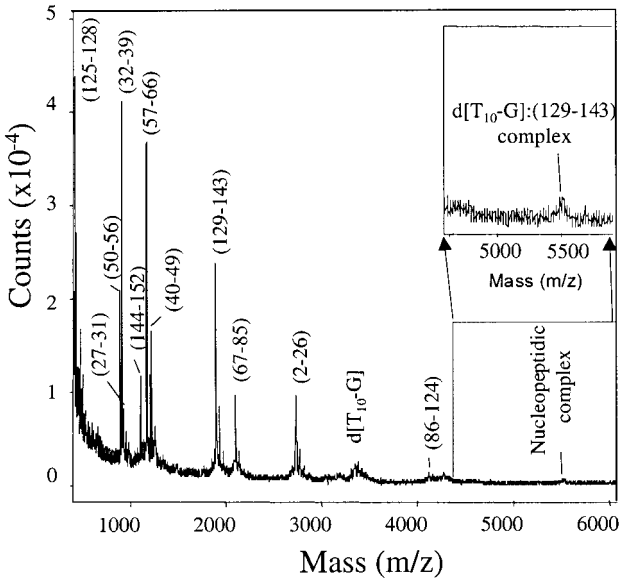

FIGURE 5: Direct MALDI-TOF analysis of a Lys-C digest of a UV laser cross-linked NDPK-B−d[T10-G] complex. Cross-linked samples of NDPK-B (6 μM) and d[T_{10}-G] (30 μM) were digested with endoproteinase Lys-C. The complete mixture was mixed with 2-ABA/NA (8:2, w/w) and spermine and analyzed via negative linear mode MALDI-TOF MS. The inset shows an expanded view of the nucleopeptidic complex peak detected only when protein was incubated with the d[T_{10}-G] after irradiation, along with potassium adducts. See Table 4 for masses.

these components (see Experimental Procedures). Altogether, these results demonstrate that peak I corresponds to a nucleopeptide and that the peptide of residues E129−K143 contains an amino acid involved in a major contact with the 11-mer oligonucleotide d[T_{10}-G].

We next analyzed the cross-linking pattern of NDPK-B and a longer oligonucleotide, using a similar protocol of separation of the nucleopeptides by RP-HPLC. Figure 7A shows the chromatogram of the Lys-C digest of the irradiated mixture of NDPK-B with a 30-mer oligonucleotide d[T_{29}-G]. Comparison with the nonirradiated mixture (not shown) indicates the presence of three new peaks denoted 15, 16, and 17 which were well resolved. These peaks exhibiting the spectral characteristics expected for nucleopeptides since their ratio of absorbency at 254 to 280 nm is close to 2 (compare the solid and dotted lines in Figure 7A) were collected and analyzed by MALDI-TOF. As shown in Figure 7B, no peak corresponding to an intact nucleopeptide complex could be detected in these three fractions. Rather, peaks corresponding to free peptides could be clearly identified in each of the three fractions. The spectra obtained from fractions 15 and 16 each contained a single major peak with an experimental mass corresponding to the peptide of residues S144−E152 (*m*/*z* 1108.5) and the peptide of residues E129−K143 (*m*/*z* 1895.2), respectively. Fraction 17 was heterogeneous and contained two different species, with a

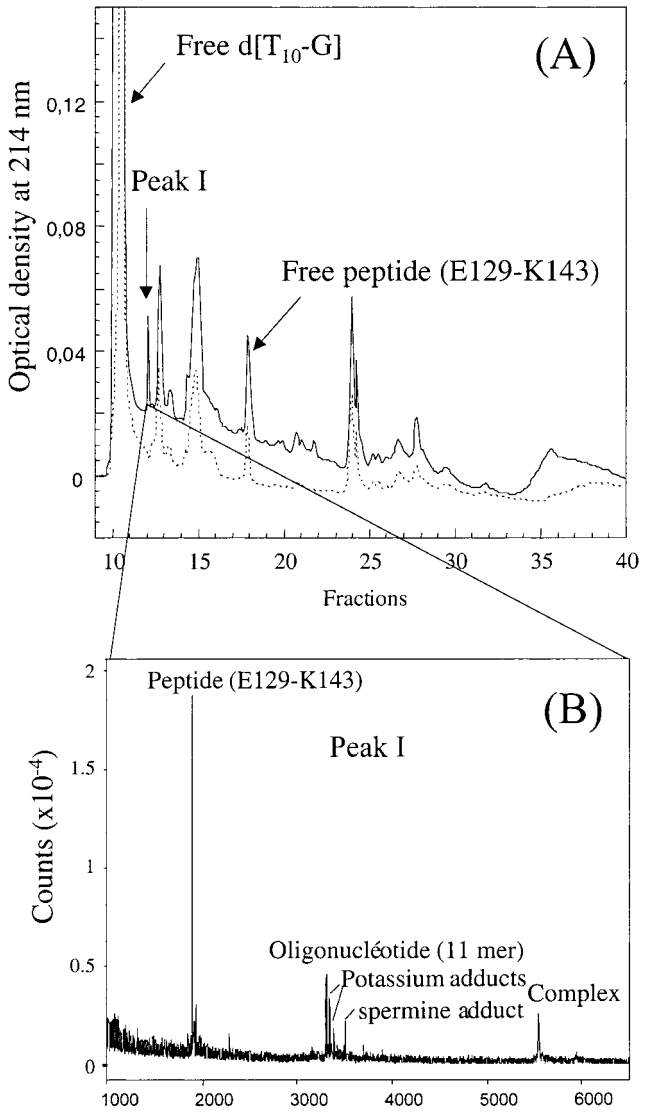

FIGURE 6: RP-HPLC purification and MALDI-TOF identification of the nucleopeptides cross-linked with d[T10-G]. (A) Samples of NDPK-B (6 μM) and d[T_{10}-G] (6 μM) irradiated (—) or not irradiated (···) were digested with endoproteinase Lys-C and separated by RP-HPLC. When the cross-linked mixture of NDPK-B and the oligonucleotide was analyzed by RP-HPLC, an additional peak (I) appeared (fraction 12). Identification by MALDI-TOF of the free peptide of residues E129−K143 (fraction 18) is shown. (B) Peak I was collected and analyzed by MALDI-TOF in the presence of 2-ABA/NA (8:2, w/w) and spermine in negative linear mode. Several adducts from potassium salts and spermine are observed on d[T_{10}-G]. Three major species were identified: peptide (residues E129−K143) at *m*/*z* 1495, d[T_{10}-G] at *m*/*z* 3307, and the cross-linked complex at *m*/*z* 5553.

major peptide of residues F40−K49 (*m*/*z* 1228.4) and a minor peptide of residues Q50−K56 (*m*/*z* 915.6). These peptides must be engaged in nucleopeptide complexes since (i) they appeared only after irradiation and (ii) the corresponding free peptides we could identify by mass spectrometry were eluted at separate positions in the chromatogram as indicated in Figure 7A. It should be noted that, despite using different matrixes, no significant peak corresponding to the d[T_{29}-G] oligonucleotide was detected in fraction 17, probably due to a high suppression effect of the peptides for the detection of d[T_{29}-G]. This effect is more drastic in terms of the signal-to-noise ratio for the sample of fraction 17 than for fractions 15 and 16.

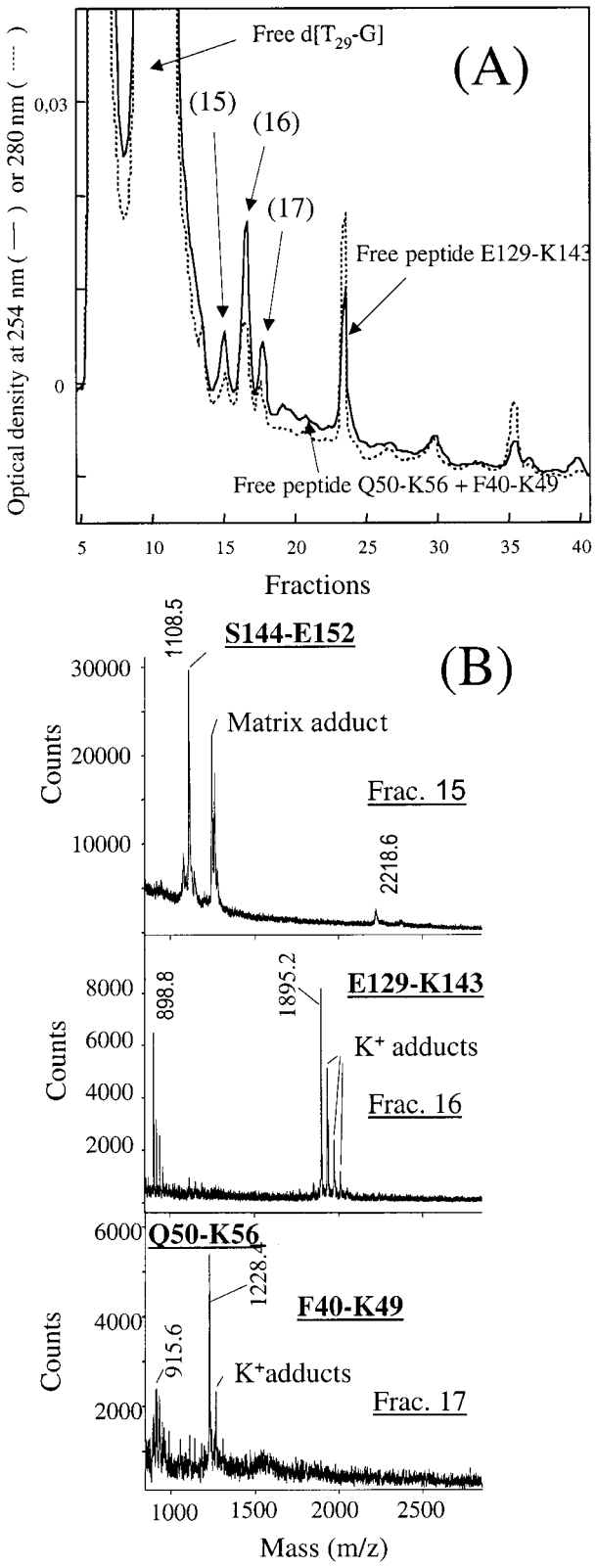

FIGURE 7: MALDI-TOF analysis of nucleopeptides cross-linked with d[T29-G]. (A) A UV laser-irradiated sample was treated as described in Experimental Procedures, and the nucleopeptides were detected by their spectroscopic properties (254 to 280 nm ratio ≈ 2) at 254 (—) and 280 nm (···). The elution volumes of the free peptides of residues E129−K143, Q50−K56, and F40−K49 resulting from protease digestion and of the free oligonucleotide are represented. (B) Fraction 15, 16, or 17 containing nucleopeptides was analyzed by MALDI-TOF in the presence of 2-ABA/NA and spermine in negative linear mode. Some potassium (K^+) and matrix (2-ABA) adducts were observed.

The results of the experiment shown in Figure 7 identify three different peptides that contact the 30-mer oligonucleotide when bound to NDPK-B. In contrast, only one cross-linked peptide was isolated when using an 11-mer (see Figures 5 and 6). This could be due either to the lack of some of the contacts when using a shorter oligonucleotide or to the relatively low sensitivity of the detection of 11-mer cross-linked peptides. Indeed, the molar absorbency of an 11-mer is considerably weaker than that of a 30-mer which could result in poor detection of the nucleopeptides eluted after RP-HPLC separation. To distinguish between these possibilities, we repeated the experiment whose results are shown in Figure 6 using a higher ratio of oligonucleotide to protein (30 μM 11-mer and 6 μM protein). The chromatogram was similar to that shown in Figure 6A except that peak I was broader (not shown). MALDI-TOF analysis of the corresponding fraction allowed identification of peptides of residues E129−K143, Q50−K56, and S144−E152. Thus, the same three distinct peptides were identified when short (11-mer) or long (30-mer) oligonucleotides were used, indicating that in both cases common peptidic determinants of the NDPK-B protein, were involved in single-strand oligonucleotide binding.

DISCUSSION

In this study, we have evaluated the binding mode of human NDPK-B to single-strand oligonucleotides and dinucleotides. By measuring the phospho-transfer enzymatic activity of NDPK-B in the presence of a series of single-strand aptamers, we show that the oligonucleotide always acts as a competitive inhibitor and therefore occupies the active site of the enzyme as previously suggested using filter binding assays (*20*). These activity measurements allowed us to calculate the inhibition constant (K_i) for each aptamer that was tested. Taking advantage of a quenching of intrinsic protein fluorescence upon oligonucleotide binding (*20*), we could also determine the dissociation constant (K_D), along with the stoichiometry of binding for the aptamer that was being considered. For all aptamers that were assayed, K_i and K_D values were consistent, although the K_D values were usually found to be ~10-fold lower than the K_i with oligonucleotides (see Table 1). This difference was less significant with dinucleotides. In addition, while the stoichiometry of binding was one per subunit for dinucleotides, only one oligomer was bound for two subunits. We interpret these results as indicating that, contrary to dinucleotides, oligonucleotides are unable to saturate simultaneously all of the six active sites within a hexameric NDPK-B (see the model shown in Figure 8).

We have shown that the presence of a guanine at the 3′-end of the 11-mer single-strand aptamer strongly increases its affinity. For example, with a K_D of 20 nM and a K_i of 170 nM, the c-*myc*−ssPu-G aptamer corresponding to one motif repeated in the NHE element from the c-*myc* promoter is by far the best inhibitor known to date for human NDPK-B catalytic activity. Kinetic studies have indicated that guanine nucleotides have a better affinity for NDP kinase as compared to other nucleotides (*2*, *3*). The structure of the complex between GDP and NDPK-B provides an explanation for this property. Indeed, the amino group of the base bound in the active site of one subunit forms hydrogen bonds to the γ-carboxylic group of the C-terminus glutamate (E152) belonging to the adjacent subunit of the same trimer within a hexamer (see also Figure 8B). The gain in affinity for an

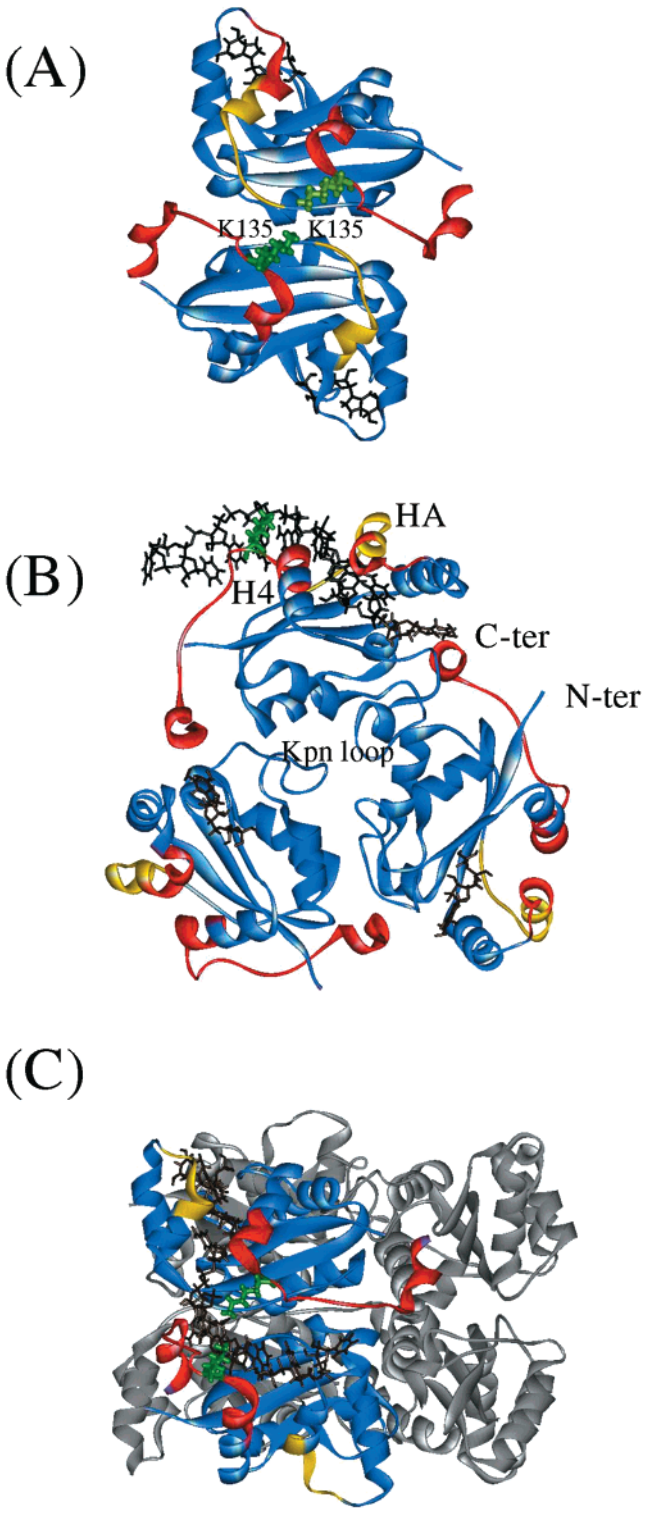

FIGURE 8: Structural model of NDPK-B bound to ssDNA. (A) Structural footprints of NDPK-B complexed with GDP and UV laser cross-linked to d[T_{29}-G] or d[T_{10}-G] (for clarity, only the dimeric unit is shown). Peptides of residues Q50−K56, E129−K143, and S144−E152, specifically cross-linked to d[T_{10}-G], are colored in red, while those cross-linked to d[T_{29}-G] are shown in red and yellow. Lys 135 is shown in green. (B and C) Structural model of NDPK-B bound to an 11-mer single-strand DNA. Views of the trimer along the 3-fold axis (B) or the hexamer along a 2-fold axis (C). The 11-mer was built using the InsightII software (Molecular Simulations) and docked to the NDPK-B according to UV laser footprints.

aptamer bearing a guanine at its 3′-end is ~10 (Table 2). It corresponds to a change in binding free energy ($\Delta\Delta G$) of 1.35 kcal/mol, a value in agreement with the possible formation of one additional hydrogen bond between a protein residue and the guanine. These results suggest that the mode of binding of the terminal base of the aptamer inside the active site of NDPK-B is similar to that of guanine in the GDP complex (see the description of the model).

Several lines of evidence point to the fact that the single-strand DNA binding activity of some NDP kinases is severely restricted and that only a few of the various isozymes of this protein found in higher organisms display DNA binding activity. Thus, Nm23-H2 only, and not Nm23-H1, was originally isolated as a transcription factor for c-*myc* (*21*). Previous results based on an electrophoretic mobility shift assay indicated that NDPK-A lacks the peptidic determinants to bind specifically to single-strand DNA (*41*). NDPK-A is a very acidic protein, while NDPK-B is a more basic protein, although they are 88% identical. In contrast, the NDP kinase from *Dictyostelium* is also very basic yet does not exhibit significant DNA binding activity (*42*). Here we show that only NDPK-B has a high binding affinity for diribonucleotides (Table 3), and for these small compounds, the polyelectrolyte effect should be negligible compared to an 11-mer or a 30-mer. We conclude that the DNA binding activity of NDPK-B is due not only to electrostatic interactions between basic residues and the phosphate backbone of DNA but also to a particular conformation of the active site of NDPK-B.

We have used an original combination of UV laser cross-linking and MALDI mass spectrometry to identify the contacts between single-strand aptamers and NDPK-B. We used UV laser nanosecond pulses, because it is sufficiently fast to "freeze" the existing equilibrium of the specific protein−nucleic acid complex, and it minimizes protein−protein cross-linking (*32*). Only one cross-linked species was obtained using an 11-mer oligonucleotide (Figure 2), and its binding affinity determined directly from the quantification of the amount of cross-linked products (0.15 μM) was very similar to the K_i measured by competition experiments (0.23 μM). Quantitative analysis of the nuclease protection assays performed with covalently bound 11-mer oligonucleotide showed that nuclease resistance was not complete. This may be due to some photo-cross-linked oligonucleotides anchored in the active site with their 3′-end exposed to the solvent.

The analysis of the peptides resulting from endoproteinase Lys-C digestion by MALDI-TOF analysis allowed us to identify three distinct peptidic footprints corresponding to peptides of residues Q50−K56, E129−K143, and S144−E152. The peptide of residues E129−K143 was the only one which could be identified directly as an intact nucleopeptide complex by MALDI without prior separation of the digested products (Figure 5). The difference between the theoretical and observed masses of the complex might result from adducts that were not resolved in linear mode, but also from the chemistry of the cross-linking itself that remains unknown. RP-HPLC of the free oligonucleotides before and after UV irradiation also showed that about 5% of the oligonucleotide was damaged, as indicated by the presence of additional peaks which may correspond to the formation of thymidine dimers (not shown) (*32*).

The peptide of residues E129−K143 is also the only one for which the precise amino acid involved in the cross-linking could be identified. Indeed, three amino acids among those composing the peptide of residues E129-E143 of NDPK-B differ in NDPK-A: S131, K135, and K143. Given the lack of binding of single-strand aptamers to NDPK-A, Lys 135 is most likely the amino acid involved in the cross-link because this residue is strictly conserved in all NDPK-Bs. In contrast, the side chain of S131 in helix H4 is pointing inside the hexamer and K143 is far from the active site inside the same subunit. So, both S131 and K143 are unlikely to make contacts with the 11-mer. Lys 135 was previously suggested to be involved in DNA binding on the basis of the analysis of the electrophoretic mobility shift assay of mutant NDPK-B (*43*). The fact that we could not visualize by MALDI-TOF spectrometry the two others nucleopeptide complexes with residues Q50−K56 and S144−E152 may result from the low stability of the complexes in solution. Little is known about the stability of the photo-cross-link, and it is likely that the dissociation occurs before the MALDI process. The fact that we never observed any complexes when nucleopeptide purification by reverse HPLC was performed under acidic conditions (0.06% TFA) supports this hypothesis.

Taken together, our results allowed us to propose a structural model for oligonucleotide bound to NDPK-B using an 11-mer d[T_{10}-G] with a guanine at its 3′-end (Figure 8). This model assumes that (i) the guanine at the 3′-end binds to the active site, stacking between F60 and V112 like the guanine of GDP in the structure of NDPK-B complexed with GDP, and (ii) a thymine from the oligonucleotide undergoes van der Waals interactions with the side chain of Lys 135. The proposed conformation for the docking of the flexible single-strand 11-mer is shown in Figure 8. It should be noted that for docking of the 11-mer oligonucleotide, we had to move helix HA away from helix H4 by about 2 Å to eliminate some sterical hindrance. The model is highly constrained, and we could not find others conformations compatible with our biochemical data. In this model, the oligonucleotide makes close contacts with both helices HA and H4 which contain three of the four peptides involved in the aptamer−protein contacts. These three peptides contain 9 of the 14 residues that differ between NDPK-B and NDPK-A. While the peptide of residues E129−K143 includes the C-terminal part of helix H4 that faces helix HA and part of the extended C-terminal end of helix H4, the peptide of residues Q50−K56 forms a part of the loop connecting helix HA and H2 and a part of helix HA (Figure 8A,B). The peptide of residues F40−K49 constitutes the major part of helix HA. It is remarkable that they are all exposed to the surface of the NDPK-B hexamer, forming a DNA-binding surface centered around the active site of one subunit. The fourth peptide (residues S144−E152) is part of the extended C-terminal segment, which is very distant from the active site within a given subunit, but it comes close to the active site of a neighboring subunit within a trimer (Figure 8B). We propose that the terminal residue composing this peptide could form hydrogen bonds with the guanine bound to the adjacent subunit. Our model applies to longer oligonucleotides such as the NHE element. In this case, it is unlikely that the oligonucleotide has its 3′-end buried in the active site like the 11-mer since the presence of a G at its

3′-end does not increase the stability of the complex (*20*). The model shown in Figure 8 provides a strong basis for our hypothesis that the molecular species interacting with the single-strand aptamer corresponds to a dimeric arrangement of the 17 kDa subunits rather than to a hexamer. Indeed, helix H4 establishes a connection between the two parts of the polypeptide chain which provide the essential contribution to the trimeric contacts and to the stability of the hexamer, i.e., the so-called "Kpn loop" and the C-terminal segment. Disruption of these contacts led to the dissociation of the hexamer in dimers (*44*). Consistent with this model is the fact that a dimeric mutant of Dd-NDPK binds to single-strand DNA while the wild-type hexameric enzyme does not (*42*). We hypothesize that the absence of several intersubunit contacts in the dimeric mutant may render helix H4 more flexible and more distant from helix HA, leading to an improved ability of the dimeric protein to accommodate the phosphate backbone and of the single-strand aptamer to bind to the active site. In addition, because double-strand DNA is less flexible and bigger than single-strand DNA, this model could explain why NDPK-B has a very poor binding activity with duplex DNA.

The similarity between the architecture of the NDP kinase fold and the subdomain of both RNA- and DNA-dependent polymerases (*5*) is of particular interest in view of the model presented in Figure 8. These proteins share a conserved domain consisting of an antiparallel β-sheet covered on one side by two α-helices. A similar $\beta\alpha\beta\beta\alpha\beta$ structural motif has been identified in several RNA binding ribonucleoproteins (RNP), such as the small nuclear ribonucleoprotein U1A bound to a 21-nucleotide RNA hairpin (*45*) or the B8 domain composing the β-subunit of phenylalanyl-tRNA synthetase which interacts specifically with the tRNA anticodon (*46*). It is remarkable that when the domain bound to the tRNA anticodon loop in protein B8 is superimposed onto our NDPK-B−ssDNA model (rmsd of 3.5 Å), the conformation of the anticodon loop of the tRNA comes very close to the single-strand 11-mer in NDPK-B (data not shown) with a similar location of the nucleic acid at the same side of the β-sheet. However, in the case of NDPK-B, helices HA and H4 come close to the β-sheet on its other side (see Figure 8B) so that the oligonucleotide is constrained. In our model, it binds within a groove formed by the catalytic active site and of the pocket located between helices HA and H4 (Figure 8A). Interestingly, this "second site" was originally proposed to bind ATP and to be the active site on the basis of a structural homology with the allosteric domain of the regulatory subunit of *E. coli* ATCase (*4*).

The heterogeneous nuclear ribonucleoprotein K (hnRNP-K) also is strikingly similar to NDPK-B. hnRNP-K was first identified as a member of a group of at least 20 major proteins constituting hnRNP particles which are presumably involved in the transport and/or processing of heterogeneous nuclear RNA and mature RNA (*52*). This protein has also been identified as a positive transcription activator for the human c-*myc* gene (*53*). Like NDPK-B, hnRNP-K specifically recognizes a single-strand cis-activating element located 100−150 bp upstream of the P1 promoter of the c-*myc* gene. The structure of the C-terminal KH module of hnRNP-K (KH3) was recently determined by NMR (*47*). Its $\beta\alpha\alpha\beta\beta\alpha$ fold, including an antiparallel β-sheet covered by three helices, is significantly similar to NDPK-B.

The biological role of NDPK-B in relation to its specific ability to bind DNA remains to be established. Apart from its role in the regulation of the transcription of the c-*myc* oncogene, a homologous NDPK from *Arabidopsis* can act as an essential transcriptional regulator in yeast (*48*). In addition, it has also been proposed that NDPK-B displays a topoisomerase activity (*28*).

The relatively low affinity of NDPK-B for double-stranded DNA, as compared to a bona fide transcription factor, and the fact that it binds preferentially to single-stranded DNA with no sequence specificity indicate that it is not a typical transcription factor. We propose that the specific binding to single-strand DNA allows NDPK-B to provide for a local increase in DNA flexibility. The creation of a single-stranded hinge would enhance the elastic properties of DNA in the NHE element of the c-*myc* gene. This increase of flexural (bending) and torsional (twisting) elasticity at this DNA site could enhance transcription by promoting the interactions between a transcription factor recognizing its cognate sequence and the basal apparatus. These interactions could not occur with the duplex DNA because of its rigidity and its periodicity. The role of NDPK-B in the regulation of transcription in cells as a nucleic acid binding protein might also be related to the protection of labile single-strand DNA or RNA against nucleases, and/or to its ability to help disrupting secondary structures such as RNA loops, formation of DNA triplex and quadruplex, which can impede transcription, and the "three R's" of genome maintenance, DNA replication, recombination, and repair.

ACKNOWLEDGMENT

We thank Dr. Malcolm Buckle at Pasteur Institute for the use of the YAG laser, Dr. Christophe Place for his help, and Professor Joël Janin for fruitful discussion.

REFERENCES

1. Agarwal, R. P., Robison, B., and Parks, R. E. J. (1978) *Methods Enzymol. 51*, 376−385.
2. Schneider, B., Xu, Y., Sellam, O., Sarfati, R., Janin, J., Veron, M., and Deville-Bonne, D. (1998) *J. Biol. Chem. 273*, 11491−11497.
3. Schaertl, S., Konrad, M., and Geeves, M. A. (1998) *J. Biol. Chem. 273*, 5662−5669.
4. Dumas, C., Lascu, I., Morera, S., Glaser, P., Fourme, R., Wallet, V., Lacombe, M.-L., Veron, M., and Janin, J. (1992) *EMBO J. 11*, 3203−3208.
5. Morera, S., Lacombe, M.-L., Xu, Y., LeBras, G., and Janin, J. (1995) *Structure 3*, 1307−1314.
6. Tepper, A., Dammann, H., Bominaar, A. A., and Veron, M. (1994) *J. Biol. Chem. 269*, 32175−32180.
7. Morera, S., Lascu, I., Dumas, C., LeBras, G., Briozzo, P., Veron, M., and Janin, J. (1994) *Biochemistry 33*, 459−467.
8. Cherfils, J., Morera, S., Lascu, I., Veron, M., and Janin, J. (1994) *Biochemistry 33*, 9062−9069.
9. Xu, Y., Sellam, O., Moréra, S., Sarfati, S., Biondi, R., Veron, M., and Janin, J. (1997) *Proc. Natl. Acad. Sci. U.S.A. 94*, 7162−7165.
10. Xu, Y., Morera, S., Janin, J., and Cherfils, J. (1997) *Proc. Natl. Acad. Sci. U.S.A. 94*, 3579−3583.
11. Mesnildrey, S., Agou, F., Karlsson, A., Deville-Bonne, D., and Veron, M. (1998) *J. Biol. Chem. 273*, 4436−4442.
12. Rosengard, A. M., Krutzsch, H. C., Shearn, A., Biggs, J. R., Barker, E., Margulies, I. M. K., King, C. R., Liotta, L. A., and Steeg, P. S. (1989) *Nature 342*, 177−180.
13. Stahl, J. A., Leone, A., Rosengard, A. M., Porter, L., King, C. R., and Steeg, P. S. (1991) *Cancer Res. 51*, 445−449.

14. Venturelli, D., Martinez, R., Melotti, P., Casella, I., Peschle, C., Cucco, C., Spampinato, G., Darzynkiewicz, Z., and Calabretta, B. (1995) *Proc. Natl. Acad. Sci. U.S.A. 92*, 7435−7439.
15. Milon, L., Rousseau-Merck, M., Munier, A., Erent, M., Lascu, I., Capeau, J., and Lacombe, M. (1997) *Hum. Genet. 99*, 550−557.
16. Munier, A., Feral, C., Milon, L., Phung-Ba Pinon, V., Gyapay, G., Capeau, J., Guellaen, G., and Lacombe, M. L. (1998) *FEBS Lett. 434*, 289−294.
17. Gilles, A. M., Presecan, E., Vonica, A., and Lascu, I. (1991) *J. Biol. Chem. 266*, 8784−8789.
18. Abdulaev, N. G., Karaschuk, G. N., Ladner, J. E., Kakuev, D. L., Yakhyaev, A. V., Tordova, M., Gaidarov, I. O., Popov, V. I., Fujiwara, J. H., Chinchilla, D., Eisenstein, E., Gilliland, G. L., and Ridge, K. D. (1998) *Biochemistry 37*, 13958−13967.
19. Wallet, V., Mutzel, R., Troll, H., Barzu, O., Wurster, B., Veron, M., and Lacombe, M.-L. (1990) *J. Natl. Cancer Inst. 82*, 1199−1202.
20. Agou, F., Raveh, S., Mesnildrey, S., and Veron, M. (1999) *J. Biol. Chem. 274*, 19630−19638.
21. Postel, E. H., Berberich, S. J., Flint, S. J., and Ferrone, C. A. (1993) *Science 261*, 478−480.
22. Berberich, S. J., and Postel, E. H. (1995) *Oncogene 10*, 2343−2347.
23. Ji, L., Arcinas, M., and Boxer, L. M. (1995) *J. Biol. Chem. 270*, 13392−13398.
24. Postel, E. H., and Ferrone, C. A. (1994) *J. Biol. Chem. 269*, 8627−8630.
25. Wells, R. D. (1988) *J. Biol. Chem. 263*, 1095−1098.
26. Mirkin, S. M., Lyamichev, V. I., Drushlyak, K. N., Dobrynin, V. N., Filippov, S. A., and Frank-Kamenetskii, M. D. (1987) *Nature 330*, 495−497.
27. Simonsson, T., and Sjoback, R. (1999) *J. Biol. Chem. 274*, 17379−17383.
28. Postel, E. H. (1999) *J. Biol. Chem. 274*, 22821−22829.
29. Kraeft, S., Traincard, F., Bourdais, J., Mesnildrey, S., Veron, M., and Chen, L. B. (1996) *Exp. Cell Res. 227*, 63−69.
30. Pinon, V. P., Millot, G., Munier, A., Vassy, J., Linares-Cruz, G., Capeau, J., Calvo, F., and Lacombe, M. L. (1999) *Exp. Cell Res. 246*, 355−367.
31. Connor, D. A., Falick, A. M., Young, M. C., and Shetlar, M. D. (1998) *Photochem. Photobiol. 68*, 299−308.
32. Hockensmith, J. W., Kubasek, W. L., Vorachek, W. R., Evertsz, E. M., and von Hippel, P. H. (1991) *Methods Enzymol. 208*, 211−236.
33. Sambrook, J., Fritsch, E. F., and Maniatis, T. (1989) *Molecular Cloning: A Laboratory Manual*, Cold Spring Harbor Laboratory Press, Cold Spring Harbor, NY.
34. Puglisi, J. D., and Tinoco, I., Jr. (1989) *Methods Enzymol. 180*, 304−325.
35. Schneider, B., Biondi, R., Sarfati, R., Agou, F., Guerreiro, C., Deville-Bonne, D., and Véron, M. (2000) *Mol. Pharmacol. 57*, 948−953.
36. Bourdais, J., Biondi, R., Lascu, I., Sarfati, S., Guerreiro, C., Janin, J., and Veron, M. (1996) *J. Biol. Chem. 271*, 7887−7890.
37. Jensen, O. N., Kulkarni, S., Aldrich, J. V., and Barofsky, D. F. (1996) *Nucleic Acids Res. 24*, 3866−3872.
38. Asara, J. M., and Allison, J. (1999) *Anal. Chem. 71*, 2866−2870.
39. Pieles, U., Zurcher, W., Schar, M., and Moser, H. E. (1993) *Nucleic Acids Res. 21*, 3191−3196.
40. Cooney, M., Czernuszewicz, G., Postel, E. H., Flint, S. J., and Hogan, M. E. (1988) *Science 241*, 456−459.
41. Hildebrandt, M., Lacombe, M.-L., Mesnildrey, S., and Veron, M. (1995) *Nucleic Acids Res. 23*, 3858−3864.
42. Mesnildrey, S., Agou, F., and Veron, M. (1997) *FEBS Lett. 418*, 53−57.
43. Postel, E. H., Weiss, V. H., Beneken, J., and Kirtane, A. (1996) *Proc. Natl. Acad. Sci. U.S.A. 93*, 6892−6897.
44. Karlsson, A., Mesnildrey, S., Xu, Y., Morera, S., Janin, J., and Veron, M. (1996) *J. Biol. Chem. 271*, 19928−19934.
45. Oubridge, C., Ito, N., Evans, P. R., Teo, C. H., and Nagai, K. (1994) *Nature 372*, 432−438.
46. Goldgur, Y., Mosyak, L., Reshetnikova, L., Ankilova, V., Lavrik, O., Khodyreva, S., and Safro, M. (1997) *Structure 5*, 59−68.
47. Baber, J. L., Libutti, D., Levens, D., and Tjandra, N. (1999) *J. Mol. Biol. 289*, 949−962.
48. Zimmermann, S., Baumann, A., Jaekel, K., Marbach, I., Engelberg, D., and Frohnmeyer, H. (1999) *J. Biol. Chem. 274*, 17017−17024.
49. Postel, E. H., Mango, S. E., and Flint, S. J. (1989) *Mol. Cell. Biol. 9*, 5123−5133.
50. Golden, M. C., Resing, K. A., Collins, B. D., Willis, M. C., and Koch, T. H. (1999) *Protein Sci. 8*, 2806−2812.
51. Urlaub, H., Thiede, B., Muller, E. C., and Wittmann-Liebold, B. (1997) *J. Protein Chem. 16*, 375−383.
52. Dreyfuss, G., Swanson, M. S., and Pinol-Roma, S. (1988) *Trends Biochem. Sci. 13*, 86−91.
53. Levens, D., Duncan, R. C., Tomonaga, T., Michelotti, G. A., Collins, I., Davis-Smyth, T., Zheng, T., and Michelotti, E. F. (1997) *Curr. Top. Microbiol. Immunol. 224*, 33−46.
54. Huang, M., Liu, S., Murray, B. K., and Lee, M. L. (1992) *Anal. Biochem. 207*, 231−235.

BI001085J